Progress in Scale Modeling, an International Journal

Volume 2 | Issue 1 Article 2

2021

Scale Model Equations and Optimization for Annular Flow of Non-Newtonian Fluids Between Eccentric and Rotating Cylinders

Wei Zhang
The Pennsylvania State University, wuz170@psu.edu

Pooya Khodaparast
The Pennsylvania State University

Amin Mehrabian Dr.
The Pennsylvania State University, amin.mehrabian@psu.edu

Amir Shojaei
Stanford University, ashojaei@slac.stanford.edu

Recommended Citation

Zhang, Wei; Khodaparast, Pooya; Mehrabian, Amin Dr.; and Shojaei, Amir (2021) "Scale Model Equations and Optimization for Annular Flow of Non-Newtonian Fluids Between Eccentric and Rotating Cylinders," *Progress in Scale Modeling, an International Journal*: Vol. 2 : Iss. 1 , Article 2.
DOI: https://doi.org/10.13023/psmij.2021.02-01-02
Available at: https://uknowledge.uky.edu/psmij/vol2/iss1/2

Scale Model Equations and Optimization for Annular Flow of Non-Newtonian Fluids Between Eccentric and Rotating Cylinders

Category

Research Article

Abstract

A broad range of engineering applications involves helical flow of non-Newtonian fluids between two eccentric cylinders. These applications often require estimation of the frictional pressure losses along the axes of the cylinders. Laboratory flow loops are commonly used to study the flow characteristics at smaller scales of investigation. This study uses the laws of similarity and dimensional analysis to obtain a set of scaling equations between the laboratory and prototype scales of the described annular flow. These equations are derived for four types of fluid rheology including Newtonian, power-law, Bingham-plastic, and yield power-law.

Results are expressed through a set of closed-form formulae that would determine the flow rate and rotational speed of the inner pipe in the laboratory model in terms of the flow rate and pipe rotation speed, as well as other flow parameters of the prototype. The specific forms of these scaling equations are developed in such a way that the dimensionless friction factors of the annular flows at the laboratory model and prototype scales become identical. In the case of the yield power-law fluid, a complete similitude between the two scales requires using a fluid in the laboratory model that is different from the prototype fluid. As such, application of the obtained equations in minimizing the laboratory flow loop size is demonstrated. It is shown that proper selection of the rheological parameters of the fluid in the flow loop model would enable substantial reduction in the geometric scale of the similitude.

Keywords

Dimensional analysis; Wellbore hydraulics; Flow loop; Rheology

Progress in Scale Modeling, an International Journal, Vol. 2, Issue 1 (2021) Article 02-01-02, pp. 1–13
https://doi.org/10.13023/psmij.2021.02-01-02

Scale Model Equations and Optimization for Annular Flow of Non-Newtonian Fluids between Eccentric and Rotating Cylinders

Wei Zhang [a], Pooya Khodaparast [a], Amin Mehrabian [a,*], Amir Shojaei [b]

[a] *The Pennsylvania State University*

[b] *SLAC National Accelerator Laboratory, Stanford University*

E-mail: amin.mehrabian@psu.edu

Received September 15, 2021, Accepted November 13, 2021

Abstract

A broad range of engineering applications involves helical flow of non-Newtonian fluids between two eccentric cylinders. These applications often require estimation of the frictional pressure losses along the axes of the cylinders. Laboratory flow loops are commonly used to study the flow characteristics at smaller scales of investigation. This study uses the laws of similarity and dimensional analysis to obtain a set of scaling equations between the laboratory and prototype scales of the described annular flow. These equations are derived for four types of fluid rheology, including Newtonian, power-law, Bingham-plastic, and yield power-law.

Results are expressed through a set of closed-form formulas that would determine the flow rate and rotational speed of the inner pipe in the laboratory model in terms of the flow rate and pipe rotation speed, as well as other flow parameters of the prototype. The specific forms of these scaling equations are developed in such a way that the dimensionless friction factors of the annular flows at the laboratory model and prototype scales become identical. In the case of the yield power-law fluid, a complete similitude between the two scales requires using a fluid in the laboratory model that is different from the prototype fluid. As such, application of the obtained equations in minimizing the laboratory flow loop size is demonstrated. The study shows that proper selection of the rheological parameters of the fluid in the flow loop model would enable substantial reduction in the geometric scale of the similitude.

Keywords: Dimensional analysis; Wellbore hydraulics; Flow loop; Rheology

Introduction

Fluid flow along the annulus between two stationary or rotating cylinders occurs in a variety of engineering applications, such as rotating tube heat exchangers [1], journal bearings [2], and circulation of drilling fluids in a subterranean well [3]. Accurate estimation of frictional pressure losses is integral to the design of such systems. Flow regime, geometry, and fluid rheology can all influence pressure loss [4, 5]. Therefore, there is a rich body of literature attempting to systematically estimate the effects of these factors on pressure loss. Solutions to laminar friction loss of power-law fluid flow in a concentric annulus with no rotation are reported in a variety of studies [6–10]. However, these solutions are not entirely straightforward because the calculations require either an iterative procedure or a numerical integration to find the radial distance across the annulus cross section at which the shear strain rate is zero [11]. In practice, the annulus may be neither concentric nor static when inner pipe rotation, vibration, and whirling occur. Therefore, fluid flow in the annulus may be helical, asymmetric, and non-stationary. The effect of these parameters either individually or in conjunction with one another is reviewed in [12]. Numerical simulation methods have been successfully applied to relax some limitations of the analytical approach [3, 13–16].

The research has since been expanded to consider more complex rheology that includes the fluid yield stress [17–19]. Yield-power law models have attracted considerable attention in the related research on

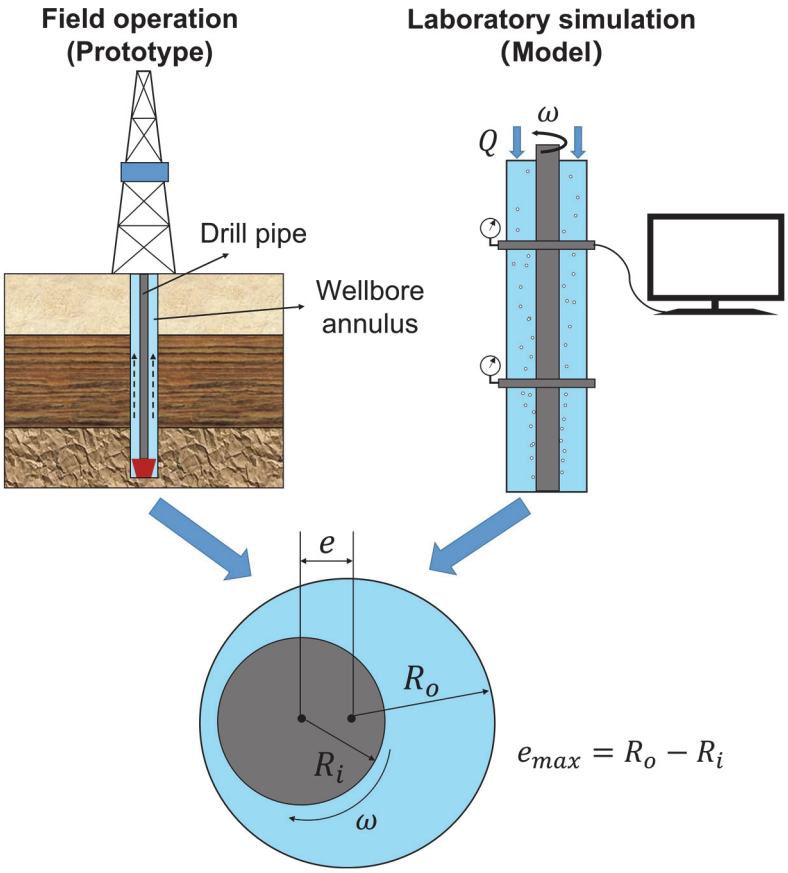

Fig. 1. Schematics of fluid flow in prototype (wellbore) and laboratory model (flow loop).

viscoelastic fluids [16, 20–22]. However, analytical solutions for the annular flow of yield power-law fluids are rarely reported in the literature. Whether solved numerically or analytically, pressure loss calculation results are commonly validated or calibrated with experiments [23–25]. Dimensional analysis is usually reserved for laboratory simulation of actual fluid flows with different space and time scales [24, 26].

This study uses dimensional analysis to obtain the scaling equations that describe complete similitude for the flow of Newtonian, power-law, Bingham-plastic, and yield power-law fluids between eccentric rotating cylinders. The dimensionless variables are identified using the Buckingham Π theorem [27]. While the developed equations are generic, the flow of drilling fluid in a wellbore annulus is a specific application. As such, the dimensional analysis aims at the direct estimation of the friction factor of the prototype (wellbore annulus) by measuring pressure gradients occurring in the laboratory model, e.g., a flow loop device.

Fig. 1 shows a laboratory setup consisting of an inner pipe simulating the drill pipe, as well as an outer pipe simulating the borehole. The quantities R_o and R_i are the radii of the outer and inner pipe, respectively, while e is the inner pipe eccentricity, ω is the angular velocity of the inner pipe, and Q is the volumetric fluid flow rate.

Full similitude between the flow loop model and the wellbore-flow prototype is attained by establishing geometric, kinematic, and dynamic similarities between the laboratory-scale and wellbore-scale flows. By taking advantage of dimensional analysis and the laws of similarity, the dimensions of the pipes, annular flow rate, and the inner pipe rotation speed in the flow loop experiment can be derived as a function of the corresponding wellbore and drill pipe dimensions, as well as the wellbore flow rate and drill pipe rotation speed.

Scaling equations

Newtonian fluids

Newtonian fluids have a constant viscosity. Fully developed flow of a Newtonian fluid in an eccentric annulus with a rotating inner pipe involves a total of 8 variables and 3 dimensions. These parameters are shown in Table 1. The quantity $\frac{\Delta p}{\Delta x}$ is the pressure gradient along the drill pipe, ρ is the fluid density, μ is the viscosity of the Newtonian fluid, U is the axial velocity of the fluid, and ω is the angular velocity of the inner pipe. Re is the Reynolds number and Ta denotes the Taylor number, while Euler's number is defined as $\mathrm{Eu} = \frac{2\Delta p}{\rho U^2}$. f is the flow friction coefficient,

Table 1. The variables, dimensions, and dimensionless parameters for Newtonian fluid case.

Group		Quantity	Expression	
Involved variables		$m = 8$	$\frac{\Delta p}{\Delta x}, \rho, \mu, R_o, R_i, e, \omega, U$	
Involved dimensions		$n = 3$	L(length), T(time), M(mass)	
Dimensionless variables $m - n = 5$	Geometric	2	Annular diameter ratio	$\frac{D_i}{D_H}$
			Dimensionless eccentricity	$\frac{e}{D_H}$
	Dynamic	3	Reynolds number, Re	$\frac{\rho U D_H}{\mu}$
			Taylor number, Ta	$\frac{\rho \omega R_i D_H}{\mu}$
			Frictional pressure loss factor, f	$\frac{D_H}{4\rho U^2}\frac{\Delta p}{\Delta x}$

which is related to Euler's number by $f = (D_H/8\Delta x)$Eu. Finally, D_H denotes a characteristic length (e.g., effective hydraulic diameter) for fluid flow which may be defined as,

$$D_H = \alpha(R_o - R_i) \tag{1}$$

where α is a dimensionless parameter. A choice of $1 < \alpha \leq 2$ is usually made in the fluid mechanics literature [28].

Aside from the eccentricity parameter, the problem involves two parameters with the dimension of length. These parameters include the outer and inner radii of the annulus: R_o and R_i. A generic definition of the problem length scale may be made through linear superposition of R_o and R_i, i.e., $D_L = \alpha_1 R_o + \alpha_2 R_i$. Any arbitrary choices of α_1 and α_2 would sustain the required geometry similarity ($\frac{D_{L,M}}{R_{o,M}} = \frac{D_{L,p}}{R_{o,P}}$ and $\frac{D_{L,M}}{R_{i,M}} = \frac{D_{L,p}}{R_{i,P}}$). The hydraulic diameter D_H defined in Eq. (1) is in fact a special value of D_L, which is obtained by setting $\alpha_1 = (-\alpha_2)$. Alternatively, selecting $\alpha_1 \neq \alpha_2 = 0$ or $\alpha_2 \neq \alpha_1 = 0$ would recover R_o or R_i as the problem length scales, respectively. The geometric dimensionless variables—namely, the hydraulic diameter ratio and the dimensionless eccentricity—measure the scaled sizes of the two pipes and the degree of inner pipe eccentricity. The Reynolds number is defined as the ratio of inertial to viscous forces of flowing fluids, while the Taylor number is the rotational counterpart of the Reynolds number. Lastly, the frictional pressure loss factor represents the ratio of the frictional pressure head gradient to the kinematic energy density of the flow.

Complete similitude requires model and prototype flows to share identical dimensionless numbers. The following similarities must be attained for this purpose:

A. Geometric similarity. This requires the length ratios between laboratory and wellbore flows to be identical, i.e.,

$$\frac{R_{i,M}}{D_{H,M}} = \frac{R_{i,P}}{D_{H,P}} \tag{2}$$

$$\frac{e_M}{D_{H,M}} = \frac{e_P}{D_{H,P}} \tag{3}$$

where subscripts M and P denote the corresponding parameters of the laboratory model and prototype flows, respectively. Therefore, ψ is introduced to represent these ratios, as follows:

$$\psi = \frac{R_{i,M}}{R_{i,P}} = \frac{R_{o,M}}{R_{o,P}} = \frac{D_{H,M}}{D_{H,P}} = \frac{e_M}{e_P} \tag{4}$$

B. Kinematic similarity. Kinematics of fluid flow in the described system is determined by two characteristic velocities attributed to the inner pipe rotation and pump flow rate. Kinematic similarity ensures that the two systems have the same ratio of these characteristic velocities in the model and prototype. This can be expressed as,

$$\eta = \frac{\omega_M R_{i,M}}{U_M} = \frac{\omega_P R_{i,P}}{U_P} \tag{5}$$

where ω is the angular velocity of the inner pipe and U is axial velocity of the fluid during annular flow, which can be calculated in turn as

$$U = \frac{Q}{\pi(R_o^2 - R_i^2)} \tag{6}$$

C. Dynamic similarity. The annular fluid Reynolds number, $\mathrm{Re} = \frac{\rho U D_H}{\mu}$, and the Taylor number, $\mathrm{Ta} = \frac{\rho \omega R_i D_H}{\mu}$, determine the flow regime. These numbers

Table 2. The variables, dimensions, and dimensionless parameters for power-law fluid case.

Group		Quantity	Expression	
Involved variables		$m = 9$	$\frac{\Delta p}{\Delta x}, \rho, R_o, R_i, e, \omega, U, K, n$	
Involved dimensions		$n = 3$	L, T, M	
Dimensionless variables $m - n = 6$	Geometric	2	Annular diameter ratio	$\frac{D_i}{D_o}$
			Dimensionless eccentricity	$\frac{e}{D_H}$
	Rheological	1	Power index	n
	Dynamic	3	Reynolds number, Re	$\frac{\rho U D_H}{\mu_{pl}}$
			Taylor number, Ta	$\frac{\rho \omega R_i D_H}{\mu_{pl}}$
			Frictional pressure loss factor, f	$\frac{D_H}{4\rho U^2}\frac{\Delta p}{\Delta x}$

must be equal in the laboratory and wellbore flows. That is,

$$\left(\frac{\rho U D_H}{\mu}\right)_M = \left(\frac{\rho U D_H}{\mu}\right)_P \tag{7}$$

and

$$\left(\frac{\rho \omega R_i D_H}{\mu}\right)_M = \left(\frac{\rho \omega R_i D_H}{\mu}\right)_P \tag{8}$$

Dividing Eq. (7) by Eq. (8) generates Eq. (5). Moreover, Q_M can be obtained after substitution from Eq. (6) into Eq. (7):

$$Q_M = Q_P \psi \left(\frac{\rho_P \mu_M}{\mu_P \rho_M}\right) \tag{9}$$

Likewise, the expression for ω_M can be obtained from Eq. (5) or Eq. (8) as follows,

$$\omega_M = \omega_P \psi^{-2} \left(\frac{\rho_P \mu_M}{\mu_P \rho_M}\right) \tag{10}$$

Complete similitude requires simultaneous geometric, kinematic, and dynamic similarities between model and prototype. Under such conditions, and according to the Buckingham Π theorem, the remaining dimensionless group of the problem, i.e., Euler's number, or alternatively the friction factor of the two flows becomes identical:

$$\frac{D_{H,M}}{4\rho_M U_M^2}\left(\frac{\Delta p}{\Delta x}\right)_M = \frac{D_{H,P}}{4\rho_P U_P^2}\left(\frac{\Delta p}{\Delta x}\right)_P \tag{11}$$

Substituting U from Eq. (6) in Eq. (11) and rearranging the mathematical terms gives

$$\begin{aligned}\left(\frac{\Delta p}{\Delta x}\right)_P &= \psi \left(\frac{\rho_P}{\rho_M}\right)\frac{U_P^2}{U_M^2}\left(\frac{\Delta p}{\Delta x}\right)_M \\ &= \psi^3 \left(\frac{\rho_M}{\rho_P}\right)\left(\frac{\mu_M}{\mu_P}\right)^{-2}\left(\frac{\Delta p}{\Delta x}\right)_M\end{aligned} \tag{12}$$

Eqs. (9), (10), and (12) determine Q_M and ω_M required for the laboratory measurement, as well as predicted pressure loss of the wellbore annular flow, $\left(\frac{\Delta p}{\Delta x}\right)_P$.

Power-law fluids

The rheology of power-law fluids is described by the consistency index K and power index n [29],

$$\tau = K\dot{\gamma}^n \tag{13}$$

where τ is shear stress and $\dot{\gamma}$ is the flow shear rate. Consequently, the apparent viscosity of the fluid can be obtained from the apparent viscosity of the power-law fluid [3, 30]:

$$\mu_{pl} = \frac{\tau}{\dot{\gamma}} \tag{14}$$

The characteristic velocity of the flow is obtained as the vector sum of the mean axial velocity and the tangential velocity at the inner pipe boundary. Similarly, the characteristic shear rate $\dot{\gamma}_F$ can be obtained by dividing the characteristic velocity by the characteristic length D_H of the annular flow:

$$\dot{\gamma} = \sqrt{\left(\frac{U}{D_H}\right)^2 + \left(\frac{\omega R}{D_H}\right)^2} \tag{15}$$

Substituting Eqs. (13) and (15) into Eq. (14)

Table 3. The variables, dimensions, and dimensionless parameters for yield power-law fluid.

Group		Quantity	Expression	
Involved variables		$m = 10$	$\frac{\Delta p}{\Delta x}, \rho, R_o, R_i, e, \omega, U, K, n, \tau_o$	
Involved dimensions		$n = 3$	L, T, M	
Dimensionless variables $m - n = 7$	Geometric	2	Annular diameter ratio	$\frac{D_i}{D_o}$
			Dimensionless eccentricity	$\frac{e}{D_H}$
	Rheological	2	Power index	n
			Hedstrom number, He	$\frac{\rho D_H^2}{\mu_{ypl}}\left(\frac{\tau_0}{\mu_{ypl}}\right)$
	Dynamic	3	Reynolds number, Re	$\frac{\rho U D_H}{\mu_{ypl}}$
			Taylor number, Ta	$\frac{\rho \omega R_i D_H}{\mu_{ypl}}$
			Frictional pressure loss factor, f	$\frac{D_H}{4\rho U^2}\frac{\Delta p}{\Delta x}$

determines the apparent viscosity of flow:

$$\mu_{pl} = K\dot{\gamma}^{n-1} = K\left(\frac{U}{D_H}\sqrt{1+\eta^2}\right)^{n-1} \tag{16}$$

The relevant variables, dimensions, and dimensionless groups of the power-law fluid flow in the annulus are summarized in Table 2. The table shows that the power index $n = n_M = n_P$ of the power-law fluid serves as the additional dimensionless parameter compared with the Newtonian fluid, while the other dimensionless groups remain the same. Consequently, an additional type of similitude—rheological similarity—is required to achieve complete similitude.

Substituting Eq. (16) into the expression for the Reynolds number from Table 2 gives

$$\mathrm{Re} = \frac{\rho U^{2-n} {D_H}^n (1+\eta^2)^{\frac{1-n}{2}}}{K} \tag{17}$$

Equality of Reynolds numbers, i.e., $\mathrm{Re}_M = \mathrm{Re}_P$, yields

$$\frac{\rho_M U_M^{2-n_M} {D_{H,M}}^{n_M} (1+\eta_M^2)^{\frac{1-n_M}{2}}}{K_M} = \frac{\rho_P U_P^{2-n_P} {D_{H,P}}^{n_P} (1+\eta_P^2)^{\frac{1-n_P}{2}}}{K_P} \tag{18}$$

Substituting U from Eq. (6) into Eq. (18) and honoring $\eta = \eta_M = \eta_P$, Eq. (18) reduces to

$$Q_M = Q_P \psi^{\frac{4-3n}{2-n}} \left(\frac{\rho_P K_M}{K_P \rho_M}\right)^{\frac{1}{2-n}} \tag{19}$$

The expression for ω_M can be immediately obtained through $\eta_M = \eta_P$:

$$\omega_M = \omega_P \psi^{-\left(\frac{2}{2-n}\right)} \left(\frac{\rho_P K_M}{\rho_M K_P}\right)^{\frac{1}{2-n}} \tag{20}$$

Finally, the equality of the friction factors (or Euler numbers) of the two flow scales yields the following equation for the wellbore pressure loss gradient:

$$\left(\frac{\Delta p}{\Delta x}\right)_P = \psi^5 \left(\frac{\rho_M}{\rho_P}\right)^{-1} \frac{Q_P^2}{Q_M^2} \left(\frac{\Delta p}{\Delta x}\right)_M = \psi^{\frac{n+2}{2-n}} \left(\frac{K_M}{K_P}\right)^{\frac{2}{n-2}} \left(\frac{\rho_M}{\rho_P}\right)^{\frac{n}{2-n}} \left(\frac{\Delta p}{\Delta x}\right)_M \tag{21}$$

Yield power-law fluids

The constitutive equation of yield power-law fluids is written as [29]

$$\tau = \tau_0 + K\dot{\gamma}^n \tag{22}$$

where τ_0 denotes yield stress. By using Eq. (14) and via a procedure similar to the case of power-law fluid, the apparent viscosity of yield power-law fluid can be formulated as

$$\mu_{ypl} = \tau_0 \dot{\gamma}^{-1} + K\dot{\gamma}^{n-1} \tag{23}$$

Table 3 shows the variables, dimensions, and dimensionless parameters for the flow of the yield power-law fluid. Compared to power-law fluids, yield power-law fluids require an additional dimensionless parameter to scale the yield stress parameter in the

Table 4. The scaling equations of similitude between the model and prototype.

Parameter	Newtonian	Power-law	Yield power-law	Bingham-Plastic
Q_r	$\psi\left(\frac{\mu_r}{\rho_r}\right)$	$\psi^{\frac{4-3n}{2-n}}\left(\frac{K_r}{\rho_r}\right)^{\frac{1}{2-n}}$	$\psi^{\frac{4-3n}{2-n}}\left(\frac{K_r}{\rho_r}\right)^{\frac{1}{2-n}}$	$\psi\frac{K_r}{\rho_r}$
ω_r	$\psi^{-2}\left(\frac{\mu_r}{\rho_r}\right)$	$\psi^{\frac{2}{n-2}}\left(\frac{K_r}{\rho_r}\right)^{\frac{1}{2-n}}$	$\psi^{\frac{2}{n-2}}\left(\frac{K_r}{\rho_r}\right)^{\frac{1}{2-n}}$	$\psi^{-2}\frac{K_r}{\rho_r}$
$\tau_{o,r}$	NA	NA	$\psi^{\frac{2n}{n-2}}K_r^{\frac{2}{2-n}}\rho_r^{\frac{n}{n-2}}$	$\psi^{-2}K_r^2\rho_r^{-1}$
$\left(\frac{\Delta p}{\Delta x}\right)_r$	$\psi^3\rho_r\mu_r^{-2}$	$\psi^{\frac{n+2}{2-n}}K_r^{\frac{2}{n-2}}\rho_r^{\frac{n}{2-n}}$	$\psi^{\frac{n+2}{2-n}}K_r^{\frac{2}{n-2}}\rho_r^{\frac{n}{2-n}}$	$\psi^3K_r^{-2}\rho_r$

constitutive relation. The Hedstrom number, He, is adopted for this purpose [31, 32]. The dimensionless group for He is expressed as

$$\mathrm{He}=\frac{\rho D_H^2}{\mu_{ypl}}\left(\frac{\tau_0}{\mu_{ypl}}\right) \tag{24}$$

Consequently, complete rheological similarity between laboratory and wellbore flows of yield power-law fluids will require equality of the corresponding Hedstrom numbers, as well as the power index n.

Likewise, substituting Eq. (15) into the expression of apparent viscosity given by Eq. (23) yields

$$\mu_{ypl}=\tau_0\left(\frac{U}{D_H}\sqrt{1+\eta^2}\right)^{-1}+K\left(\frac{U}{D_H}\sqrt{1+\eta^2}\right)^{n-1} \tag{25}$$

The Reynolds number is rewritten in terms of flow rate as

$$\mathrm{Re}=\frac{\frac{\rho Q^2}{\pi^2(R_o^2-R_i^2)^2}\sqrt{1+\eta^2}}{\tau_0+K\left[\frac{Q\sqrt{1+\eta^2}}{\pi(R_o^2-R_i^2)D_H}\right]^n} \tag{26}$$

Subsequently, the appropriate values for flow rate and angular velocity can be obtained by simultaneous application of the equations

$$\mathrm{Re}_M=\mathrm{Re}_P \tag{27}$$

and

$$\mathrm{He}_M=\mathrm{He}_P \tag{28}$$

Substituting the expressions of Re and He into Eq. (27) and (28) then simultaneously solving Eqs. (27) and (28) give two new equations:

$$Q_M=Q_P\psi^{\frac{4-3n}{2-n}}\left(\frac{K_M\rho_P}{K_P\rho_M}\right)^{\frac{1}{2-n}} \tag{29}$$

and

$$\tau_{0,M}=\psi^{-\frac{2n}{2-n}}\left(\frac{K_M}{K_P}\right)^{\frac{2}{2-n}}\left(\frac{\rho_M}{\rho_P}\right)^{\frac{n}{n-2}}\tau_{0,P} \tag{30}$$

By securing the kinematic similarity condition $\eta_M=\eta_P$ from Eq. (5), the expression for ω_M is obtained as

$$\omega_M=\psi^{-\left(\frac{2}{2-n}\right)}\left(\frac{K_M\rho_P}{K_P\rho_M}\right)^{\frac{1}{2-n}}\omega_P \tag{31}$$

Interestingly, the expressions of Q_M and ω_M for the yield power-law fluid are the same as the power-law case but with an additional constraint for yield stress of the experimental model $\tau_{0,M}$, as obtained in Eq. (30).

Finally, $\left(\frac{\Delta p}{\Delta x}\right)_P$ can be obtained through equality of friction factors as follows:

$$\left(\frac{\Delta p}{\Delta x}\right)_P=\psi^{\frac{n+2}{2-n}}\left(\frac{K_M}{K_P}\right)^{\frac{2}{n-2}}\left(\frac{\rho_M}{\rho_P}\right)^{\frac{n}{2-n}}\left(\frac{\Delta p}{\Delta x}\right)_M \tag{32}$$

The Bingham-plastic fluid is a special case of the yield power-law fluid where in Eq. (22), $n=1$ [29, 33]. Therefore, the scaling equations for Bingham-plastic fluid can be obtained by setting $n=1$ in Eqs. (29) through (32). A summary of the scaling equations between the model and prototype parameters for the considered fluid rheologies is outlined in Table 4. Here, the ratios of each parameter are defined as $Q_r=\frac{Q_M}{Q_P}$, $\omega_r=\frac{\omega_M}{\omega_P}$, $\tau_{0,r}=\frac{\tau_{0,M}}{\tau_{0,P}}$, $\mu_r=\frac{\mu_M}{\mu_P}$, $\rho_r=\frac{\rho_M}{\rho_P}$, and $K_r=\frac{K_M}{K_P}$, while the pressure loss gradient ratio is defined as $\left(\frac{\Delta p}{\Delta x}\right)_r=\left(\frac{\Delta p}{\Delta x}\right)_p/\left(\frac{\Delta p}{\Delta x}\right)_M$.

Verification of the scaling equations

The obtained scaling equations are verified against existing analytical solutions for the pertinent special case problems involving annular or pipe flow of various fluid rheologies. The following solutions are considered

for this purpose:

- Analytical solution for laminar flow of Newtonian fluids in an eccentric annulus [34]; It can be verified that Eq. (12) of the current work can be obtained by comparing the lab-scale and wellbore-scale pressure loss gradients using the results of [34].
- Analytical solution for laminar flow of a power-law fluid in a concentric annulus [7]; this solution conforms with Eqs. (19) and (21) of the current work.
- Analytical solution for the laminar flow of yield power-law fluids in a pipe [28]; Eqs. (29) and (32) of the current scaling model can be validated against this solution [28].
- Analytical solution for laminar flow of yield power-law fluids and Bingham-Plastic fluids in a rotational viscometer [35]; Eqs. (30) and (31) of the presented similitude model are consistent with their solution [35].

The detailed derivations for the above-outlined verifications are presented in the Appendix.

Discussion of the results

The ratios Q_r, ω_r, and $\tau_{0,r}$ are the main design parameters of the laboratory-scale model device. The following equation may be obtained by evaluating the ratios between Eqs. (29) and (31):

$$\frac{Q_r}{\omega_r} = \frac{Q_M/Q_P}{\omega_M/\omega_P} = \psi^3 \tag{33}$$

The same equation can also be obtained by dividing Eq. (9) with Eq. (10). Therefore, the equation applies to all fluid rheology types.

Eq. (33) denotes a compromise between the flow rate Q_M and inner pipe rotation speed ω_M if the objective is to keep the flow loop device size in check. That is to say that a small model device (small ψ) would require small Q_M and large ω_M. The former is a favorable factor in designing the laboratory setup since it allows for using a smaller pump. The latter, however, could impose practical restrictions on the size of the flow loop device since the rotation speed of the device inner pipe cannot grow arbitrarily large.

Flow of noncolloidal suspension of particles in yield power-law fluids

An aspect of the conducted dimensional analysis is to properly select the fluid rheology of the experimental model. The dimensional analysis presented in the previous section indicates that the scaling of the equations for the flow of a yield-power law fluid is generally possible. However, such a scaling requires using a different fluid in the laboratory model than the prototype. A potential challenge of such a scaling practice for yield power-law fluids is that the relations among the fluid rheological parameters—k, n and τ_0—are rather entangled. Existing predictive models for such relations are scant in the literature.

A rare case might be noncolloidal suspension of particles in a yield power-law fluid, which is herein considered to further explain the practical implications of the presented scaling equations. The suspension flow of a drilling fluid mixed with solid-particle additives, such as weighting agents as well as drill cuttings, in a wellbore annulus is an example of such a system [36]. The total volume fraction of solids in the wellbore fluid is ϕ_P. The fluid used in the laboratory model is assumed to be the decontaminated wellbore fluid from which the solids are partially removed at the surface facilities of the drilling rig to a new volume fraction, $\phi_M < \phi_P$ [37]. Ovarlez, et al. [38] obtained the consistency index and yield stress of a suspension system in terms of the volume fraction of solid particles, ϕ, in the mixture. These relations can be rearranged to obtain the desired parameter ratios as follows:

$$K_r(\phi_M, \phi_P) = \left[\frac{(1-\phi_M/\phi_{div})^{-(5/2)(n+1)\phi_{div}}(1-\phi_M)^{(1-n)}}{(1-\phi_P/\phi_{div})^{-(5/2)(n+1)\phi_{div}}(1-\phi_P)^{(1-n)}}\right]^{\frac{1}{2}} \tag{34}$$

and

$$\tau_{0,r}(\phi_M, \phi_P) = \left[\frac{1-\phi_M(1-\phi_M/\phi_{div})^{-(5/2)\phi_{div}}}{1-\phi_P(1-\phi_P/\phi_{div})^{-(5/2)\phi_{div}}}\right]^{\frac{1}{2}} \tag{35}$$

where ϕ_{div} is the maximum packing fraction of the suspension flow. A value of $\phi_{div} = 0.605$ is recommended in [38]. Here, $K_r(\phi) = \frac{K_M}{K_P}$ and $\tau_{0,r}(\phi) = \frac{\tau_{0,M}}{\tau_{0,P}}$ are the ratios of the fluid consistency index and yield stress at the model and prototype scales. Further, the density of the suspension can be formulated as

$$\rho_r(\phi) = \frac{\phi_M\rho_{s,r} + (1-\phi_M)}{\phi_P\rho_{s,r} + (1-\phi_P)} \tag{36}$$

where $\rho_{s,r} = \frac{\rho_s}{\rho_0}$ in which ρ_0 is the density of the clean fluid with no suspended solids. Likewise, $\rho_r = \frac{\rho_M}{\rho_P}$ is the ratio of the model fluid density to the fluid density. An equation for the required geometric scale of the laboratory model can be obtained by solving Eq. (30) for ψ after substitution from Eqs. (34) into (36). The resulting expression is written as

$$\psi(\phi_P, \phi_M) = \left(\frac{1-\phi_P}{1-\phi_M}\right)^{1/4}\left(\frac{\phi_{div}-\phi_M}{\phi_{div}-\phi_P}\right)^{-15\phi_{div}/8}\left[\frac{1+\phi_P(\rho_{s,r}-1)}{1+\phi_M(\rho_{s,r}-1)}\right]^{\frac{1}{2}} \tag{37}$$

Interestingly, the obtained scaling ratio is independent

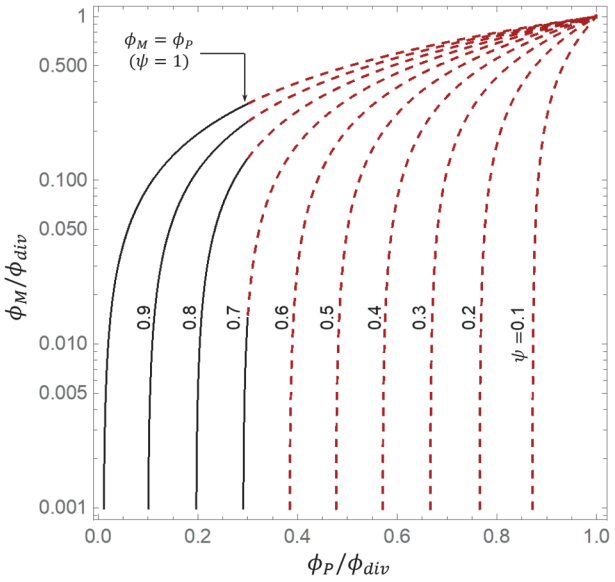

Fig. 2. Variation of the model scale ψ with normalized solid content of the wellbore fluid.

of the fluid power index, n. Fig. 2 shows the contour plots of the laboratory model geometric scale ψ versus the normalized solids content of the drilling fluid in the wellbore and the laboratory model. The portion of plot curves pertaining to $\phi_P > 0.2$ is presented in dashed format since in practice the solid volume fraction in the wellbore fluid does not exceed 20% [37]. The plot indicates that for this range of ϕ_P, a substantial reduction in the scaled size of the wellbore annulus is not feasible when the same base fluid as the wellbore fluid is used in the model. This result further stresses the necessity for design and synthesis of alternative fluid chemistry and rheology when aiming for small experimental models of non-Newtonian flow systems. The design optimization scheme which is presented in the following section explores such a possibility.

Optimization of experimental model design based on model fluid rheology

A mathematical problem can be formulated in order to obtain the optimal values of a similitude design. By taking the logarithm of Eqs. (29), (30), and (31), the following linear system of equations can be obtained

$$\begin{bmatrix}\log\tau_{0r}\\ \log\omega_r\\ \log Q_r\end{bmatrix} = \frac{1}{2-n}\begin{bmatrix}2n & 2 & -2\\ -2 & 1 & -1\\ 4-3n & 1 & -1\end{bmatrix} \cdot \begin{bmatrix}\log\psi\\ \log K_r\\ \log\rho_r\end{bmatrix} \tag{38}$$

where the subscript r denotes the ratio of a laboratory model value to the corresponding prototype value, e.g., $\omega_r = \frac{\omega_M}{\omega_P}$. If a similitude design based on selected values of (ψ, K_r, ρ_r) is considered, the set of values for τ_{0r}, ω_r and Q_r can be obtained correspondingly. A practical challenge of such a design is that the rheological set of parameters ρ, τ_0 and K are interdependent through the designed fluid chemistry, not the scaling laws of mechanics. Therefore, it is not straightforward, if even possible, to adjust the yield stress of a fluid after the other rheological properties (K, ρ, n) are set at given values. Resultingly, a similitude design based solely on the fluid rheology appears to be more feasible. In this aspect, the following rearrangement of the matrix relation in Eq. (38) is considered:

$$\begin{bmatrix}\log\psi\\ \log\omega_r\\ \log Q_r\end{bmatrix} = \frac{1}{2n}\begin{bmatrix}-(2-n) & 2 & -n\\ 2 & -2 & 0\\ -(4-3n) & 4 & -3n\end{bmatrix} \cdot \begin{bmatrix}\log\tau_{0r}\\ \log K_r\\ \log\rho_r\end{bmatrix} \tag{39}$$

From an operational standpoint, the experimental model design aims at minimizing the geometric ratio ψ and laboratory flow rate Q_M. The rotational speed ω_M is constrained by an upper threshold based on the available motor speeds and consideration of the inner pipe vibrations. Given the designed fluid chemistry, certain box constraints for rheological quantities $(\tau_{0,M}, K_M, \rho_M)$ may apply. The optimization problem at hand may be mathematically formulated as follows. The objective is to find a vector $\mathbf{x} = [\log\tau_{0r} \quad \log K_r \quad \log\rho_r]^T$ that minimizes

$$\begin{aligned} f(\mathbf{x}) &= \beta\log\psi + (1-\beta)\log Q_r \\ &= \frac{1}{2n}[\beta \quad (1-\beta)] \\ &\quad \cdot \begin{bmatrix}-(2-n) & 2 & -n\\ -(4-3n) & 4 & -3n\end{bmatrix}\cdot\mathbf{x} \end{aligned} \tag{40}$$

when subjected to the following constraint for the inner pipe speed,

$$\log\omega_r = \frac{1}{2n}[2 \quad -2 \quad 0]\cdot\mathbf{x} \le \log\omega_{r,\max} \tag{41}$$

and a set of box constraints for fluid rheology parameters, including

$$\mathbf{x}_{\min} \le \mathbf{x} \le \mathbf{x}_{\max} \tag{42}$$

in which

$$\mathbf{x}_{\min} = [\log\tau_{0r,\min} \quad \log K_{r,\min} \quad \log\rho_{r,\min}]^T \tag{43}$$

and

$$\mathbf{x}_{\max} = [\log\tau_{0r,\max} \quad \log K_{r,\max} \quad \log\rho_{r,\max}]^T \tag{44}$$

The quantity β in Eq. (40) is a weighting factor for this optimization [39]. Linear programming [40] can be applied to obtain the solution to optimization problem as outlined by Eqs. (40) to (44). The solution is independent of the weighting parameter β, which can

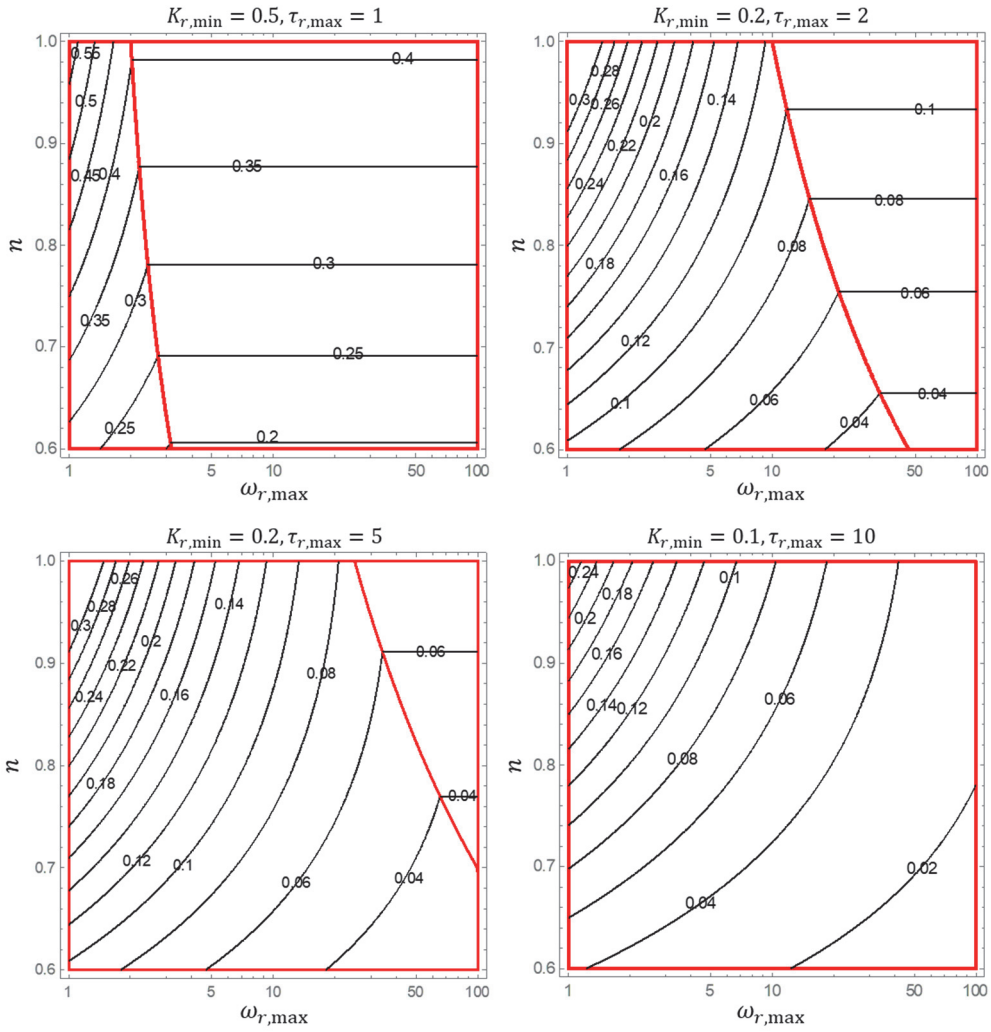

Fig. 3. Contour plots of the optimized solution for minimum scaling ratio ψ as a function of $1 < \omega_{r,\max} < 100$ on a log scale on the horizontal axis and $0.6 \le n \le 1$ on the vertical axis. Here, $\rho_{max} = 1.5$.

be expressed as follows,

$$\mathbf{x} = \left[\log\left\{\min\left[K_{r,\min}\omega_{r,\max}^{n}, \tau_{0r,\max}\right]\right\} \quad \log K_{r,\min} \quad \log \rho_{r,\max}\right]^{T} \tag{45}$$

Substitution of Eq. (45) into Eq. (39) yields

$$\psi_{\min} = \begin{cases} \omega_{\mathrm{r,max}}^{-n}\left(\dfrac{K_{\mathrm{r,min}}}{\rho_{\mathrm{r,max}}}\right)^{\frac{(2-n)}{2n}} & K_{r,\min}\omega_{r,\max}^{n} < \tau_{r,\max} \\ \dfrac{K_{\mathrm{r,min}}^{1/n}}{\tau_{\mathrm{r,max}}^{1/2}\,\rho_{\mathrm{r,max}}^{[(2-n)/2n]}} & K_{r,\min}\omega_{r,\max}^{n} \ge \tau_{r,\max} \end{cases} \tag{46}$$

Consequently, substituting Eq. (46) in Eq. (33) determines the model flow rate as follows:

$$Q_{\mathrm{M,min}} = \left(\frac{\psi_{\min}^{3}\omega_{M,\max}}{\omega_{P}}\right) Q_{P} \tag{47}$$

Fig. 3 displays the optimized solution given by Eq. (46). The horizontal axis in the plots is the maximum rotational speed ratio $\omega_{r,\max}$, while the vertical axis denotes the fluid power index n. The assumed values for the consistency index ratio $K_{r,\min}$ and the yield stress ratio $\tau_{0r,\max}$ of each plot are displayed. The inner red boundary within the plots represents the locus of discontinuity points on each contour curve. This boundary can be represented by the following equation:

$$\omega_{r,\max} = \left(\frac{\tau_{r,\max}}{K_{r,\min}}\right)^{1/n} \tag{48}$$

Fig. 3 demonstrates that a higher rotational speed and a smaller power index allows for selecting a smaller scaling ratio, ψ. However, if the rotational speed reaches the threshold defined by Eq. (43), the minimum scaling ratio is only a function of the fluid power index.

Conclusions

Dimensional analysis is used to develop a set of scaling equations between the experimental model and prototype for non-Newtonian fluid flows along the annulus of rotating cylinders. The flow rate, inner pipe rotation speed, and fluid rheology of the scaled model are selected in such a way that full similitude between the two scales of flow is achieved. The following conclusions are drawn:

1. For all the considered fluid types, the scaled values for the flow rate Q_M and pipe rotational speed ω_M of the laboratory model are linearly proportional to the corresponding parameters of the wellbore-scale prototype, i.e., Q_P and ω_P. The proportionality constant depends on the length ratio ψ, density ratio $\frac{\rho_M}{\rho_P}$, consistency index ratio $\frac{K_M}{K_P}$, and power index n.
2. The scaling expressions for Q_M and ω_M for yield power-law fluids are the same as the power-law fluid. However, achieving complete similitude requires an additional constraint on the yield stress $\tau_{0,M}$ of the laboratory fluid.
3. A fluid with smaller consistency index and larger yield stress, as well as higher rotational speed of the inner cylinder, serves to reduce the size of the scaled experimental model.

Appendix A. Verification against the existing analytical solutions

Flow of Newtonian fluids through an eccentric annulus

Piercy et al. [34] derived the relationship between pressure loss gradient and pumping rate for laminar flow of Newtonian fluids in an eccentric annulus without inner pipe rotation. The derived equations are outlined as follows:

$$\frac{dp}{dx} = -\frac{8\mu Q}{\pi}\left[R_o^4 - R_i^4 - \frac{4e^2M^2}{B-A} - 8e^2M^2\sum_{i=1}^{\infty}\frac{i\exp[-i(B+A)]}{\sinh(iB-iA)}\right]^{-1} \quad \text{(A1)}$$

$$M = (F^2 - R_o^2)^{\frac{1}{2}} \quad \text{(A2)}$$

$$F = \frac{R_o^2 - R_i^2 + E^2}{2\mathrm{E}} \quad \text{(A3)}$$

$$A = \frac{1}{2}\ln\left(\frac{F+M}{F-M}\right) \quad \text{(A4)}$$

and

$$B = \frac{1}{2}\ln\left(\frac{F-E+M}{F-E-M}\right) \quad \text{(A5)}$$

The parameters with a length dimension can be written in terms of a constant multiplied by the outer radius as

$$R_i = C_1 R_o \quad \text{(A6)}$$

and

$$e = C_2 R_o \quad \text{(A7)}$$

Substituting into Eq. (A1) gives

$$\frac{dp}{dx} = -\frac{8\mu Q}{\pi R_o^4}\left[1 - C_1^4 - \frac{4C_2^2M'^2}{B-A} - 8C_2^2M'^2\sum_{i=1}^{\infty}\frac{i\exp[-i(B+A)]}{\sinh(iB-iA)}\right]^{-1} \quad \text{(A8)}$$

$$M' = (F^2 - R_o^2)^{0.5} = \left[\left(\frac{1 - C_1^2 + C_2^2}{2\mathrm{C}_2}\right)^2 - 1\right]^{\frac{1}{2}} \quad \text{(A9)}$$

$$F' = \frac{R_o^2 - R_i^2 + E^2}{2\mathrm{E}} = \frac{1 - C_1^2 + C_2^2}{2C_2} \quad \text{(A10)}$$

$$A = \frac{1}{2}\ln\left(\frac{F'+M'}{F'-M'}\right) \quad \text{(A11)}$$

and

$$B = \frac{1}{2}\ln\left(\frac{F'-E'+M'}{F'-E'-M'}\right) \quad \text{(A12)}$$

The geometric similarity between laboratory and prototype conditions indicates that the two scales have the same values for C_1 and C_2. This also indicates that the two scales share the same values for M', F', A, and B. Therefore, the following relationship can be obtained from Eq. (A8):

$$\frac{\left(\frac{dp}{dx}\right)_M}{\left(\frac{dp}{dx}\right)_P} = \psi^{-4}\frac{\mu_M}{\mu_P}\frac{Q_M}{Q_P} \quad \text{(A13)}$$

The same relationship can be readily attained by combining Eqs. (9) and (12) of the current work. Therefore, the proposed solution for the Newtonian fluid case is consistent with the analytical solution outlined in [34].

Flow of Power-law fluids through a concentric annulus

The following analytical solution for laminar flow of power-law fluid in a non-rotating and concentric annulus was proposed by Fredrickson and Bird [7]

$$Q = \frac{n}{3n+1}\pi R_o^{\frac{3n+1}{n}}\left(\frac{1}{2K}\frac{dp}{dx}\right)^{\frac{1}{n}}\left[(1-\beta^2)^{1+\frac{1}{n}} - \kappa^{1-\frac{1}{n}}(\beta^2-\kappa^2)^{1+\frac{1}{n}}\right] \quad \text{(A14)}$$

The parameter β can be determined from the following integral equation

$$\int_{\kappa}^{\beta}\left(\frac{\beta^2}{\xi}-\xi\right)^{\frac{1}{n}}d\xi=\int_{\beta}^{1}\left(\xi-\frac{\beta^2}{\xi}\right)^{\frac{1}{n}}d\xi \tag{A15}$$

where $\xi=\frac{r}{R_o}$ is the dimensionless radial coordinate and $\kappa=\frac{R_i}{R_o}$ is the dimensionless inner radius.

The quantity β in Eq. (A15) is only a function of ξ and κ. The laboratory model and prototype share the same values of ξ and κ due to geometric similarity. Therefore, Eq. (A14) can be used to obtain

$$\frac{Q_M}{Q_P}=\psi^{\frac{3n+1}{n}}\left(\frac{K_M}{K_P}\right)^{-\frac{1}{n}}\left[\frac{\left(\frac{dp}{dx}\right)_M}{\left(\frac{dp}{dx}\right)_P}\right]^{\frac{1}{n}} \tag{A16}$$

Eq. (A16) agrees with Eqs. (19) and (21) of the current work.

Flow of yield power-law fluids through a pipe

The relation between axial velocity and pressure loss gradient for laminar flow of the yield power-law fluids in a static pipe is derived in [28]. The result is expressed through the following closed-form equation

$$U=\frac{R_o(\tau_w-\tau_0)^{\frac{n+1}{n}}}{4K^{\frac{1}{n}}\tau_w^3}\left(\frac{4n}{3n+1}\right)\left[\tau_w^2+\frac{2n}{1+2n}\tau_0\tau_w+\frac{2n^2}{(1+n)(1+2n)}\tau_0^2\right] \tag{A17}$$

where the shear stress at the pipe wall τ_w is

$$\tau_w=\frac{R}{2}\frac{\Delta p}{\Delta x} \tag{A18}$$

Therefore, the volumetric flow rate becomes

$$Q=\frac{\pi R_o^3(\tau_w-\tau_0)^{\frac{n+1}{n}}}{4K^{\frac{1}{n}}\tau_w^3}\left(\frac{4n}{3n+1}\right)\left[\tau_w^2+\frac{2n}{1+2n}\tau_0\tau_w+\frac{2n^2}{(1+n)(1+2n)}\tau_0^2\right] \tag{A19}$$

Consequently, the ratio between laboratory and prototype flow rates can be expressed as follows:

$$\frac{Q_M}{Q_P}=\frac{\psi^3\left[\frac{(\tau_w-\tau_0)_M}{(\tau_w-\tau_0)_P}\right]^{\frac{n+1}{n}}}{\left(\frac{K_M}{K_P}\right)^{\frac{1}{n}}\left[\frac{\tau_{w,M}}{\tau_{w,P}}\right]^3}\frac{\left[\tau_w^2+\frac{2n}{1+2n}\tau_0\tau_w+\frac{2n^2}{(1+n)(1+2n)}\tau_0^2\right]_M}{\left[\tau_w^2+\frac{2n}{1+2n}\tau_0\tau_w+\frac{2n^2}{(1+n)(1+2n)}\tau_0^2\right]_P} \tag{A20}$$

Substituting Eq. (A18) into Eq. (A20) gives

$$\frac{Q_M}{Q_P}=\frac{\left[\frac{\frac{R_M}{2}-\frac{\tau_{0,M}}{\left(\frac{\Delta p}{\Delta x}\right)_M}}{\frac{R_P}{2}-\frac{\tau_{0,P}}{\left(\frac{\Delta p}{\Delta x}\right)_P}}\right]^{\frac{n+1}{n}}}{\left(\frac{K_M}{K_P}\right)^{\frac{1}{n}}\left[\frac{\left(\frac{\Delta p}{\Delta x}\right)_M}{\left(\frac{\Delta p}{\Delta x}\right)_P}\right]^{-\frac{1}{n}}}\frac{\frac{R_{o,M}^2}{4}+\frac{2n}{1+2n}\frac{R_{o,M}}{2}\frac{\tau_{0,M}}{\left(\frac{\Delta p}{\Delta x}\right)_M}+\frac{2n^2}{(1+n)(1+2n)}\frac{\tau_{0,M}^2}{\left(\frac{\Delta p}{\Delta x}\right)_M^2}}{\frac{R_{o,P}^2}{4}+\frac{2n}{1+2n}\frac{R_{o,P}}{2}\frac{\tau_{0,P}}{\left(\frac{\Delta p}{\Delta x}\right)_P}+\frac{2n^2}{(1+n)(1+2n)}\frac{\tau_{0,P}^2}{\left(\frac{\Delta p}{\Delta x}\right)_P^2}} \tag{A21}$$

Dividing Eq. (30) by Eq. (32) leads to the following equation:

$$\frac{\tau_{0,M}}{\left(\frac{\Delta p}{\Delta x}\right)_M}=\psi\frac{\tau_{0,P}}{\left(\frac{\Delta p}{\Delta x}\right)_P} \tag{A22}$$

Substituting Eq. (A22) into Eq. (A21) yields

$$\frac{Q_M}{Q_P}=\psi^{\frac{3n+1}{n}}\left(\frac{K_M}{K_P}\right)^{-\frac{1}{n}}\left[\frac{\left(\frac{\Delta p}{\Delta x}\right)_M}{\left(\frac{\Delta p}{\Delta x}\right)_P}\right]^{\frac{1}{n}} \tag{A23}$$

Eq. (A23) is consistent with Eqs. (29) and (32) of the current work.

Flow of yield power-law fluids between rotating cylinders

Chatzimina et al. [35] presented the solution of angular speed for the flow of yield power-law fluids in a rotational flowmeter with a rotating inner pipe, the dimensionless angular speed for the fluid $U_{\theta D}$ was solved to be

$$U_{\theta D}(r_D)=\left[1-\mathrm{Bn}^{\frac{1}{n}}\int_1^{r_D}\frac{1}{\xi}\left(\frac{c}{\xi}-1\right)^{\frac{1}{n}}d\xi\right]r_D \tag{A24}$$

where

$$U_{\theta D}=\frac{U_\theta}{\omega R_i} \tag{A25}$$

$$\mathrm{Bn}=\frac{\tau_0}{K\omega^n} \tag{A26}$$

and

$$r_D=\frac{r}{R_i} \tag{A27}$$

The parameter c can be solved from

$$\mathrm{Bn}^{\frac{1}{n}} = \frac{1}{\int_1^{R_{oD}} \frac{1}{\xi}\left(\frac{c}{\xi}-1\right)^{\frac{1}{n}} d\xi} \tag{A28}$$

with the dimensionless outer radius defined as $R_{oD} = \frac{R_o}{R_i}$.

As can be seen, constant c is a function of R_{oD}, Bn, and n. By dividing Eq. (30) by Eq. (31) to the power of n, the following result is achieved:

$$(\mathrm{Bn})_M = (\mathrm{Bn})_P \tag{A29}$$

Due to the rheological and geometrical similarity, the following equations can also be found:

$$R_{oD,M} = R_{oD,P} \tag{A30}$$

and

$$n_M = n_P \tag{A31}$$

Therefore, the two scales also share the same constant $c_M = c_P$, which indicates that the prototype and the model achieve dynamic similarity, i.e., the two scales have the same dimensionless angular speed when the dimensionless radius is equal.

Reversely, this work shows that when the two scales achieve dynamic similarity, Eq. (A24) is also consistent with the current work. If the prototype and the model achieve dynamic similarity, the two scales should have the same dimensionless angular speed when the dimensionless radius is equal:

$$U_{\theta D,M}(r_D) = U_{\theta D,P}(r_D) \tag{A32}$$

Eq. (A32) implies the similarity of the tangential velocity profiles, i.e., a complete similitude between the model and prototype.

Flow of Bingham-plastic fluids in a rotating annulus

Chatzimina et al. [35] presented the closed-form solution of angular speed for the flow of Bingham-plastic fluids in a rotational flowmeter with a rotating inner pipe. The dimensionless angular speed of the fluid $U_{\theta D}$ is reported in [35] as follows:

$$U_{\theta D}(r_D) = \left\{1 + \left[\mathrm{Bn}\ln r_D + \frac{R_{oD}^2}{R_{oD}^2-1}(\mathrm{Bn}\ln R_{oD} + 1)\left(\frac{1}{r_D^2}-1\right)\right]\right\} r_D \tag{A33}$$

The advantage of Eq. (A33) over Eq. (A24) is the explicit form of the mathematical expression for the tangential velocity. Therefore, a comparison with the scale model equations of this paper would be more straightforward. The kinematic similarity between the two scales of flow requires identical values of dimensionless angular speed at a given r_D. The following equation can subsequently be deduced from Eq. (A33):

$$\left[\mathrm{Bn}\ln r_D + \frac{R_{oD}^2}{R_{oD}^2-1}(\mathrm{Bn}\ln R_{oD} + 1)\left(\frac{1}{r_D^2}-1\right)\right]_M = \left[\mathrm{Bn}\ln r_D + \frac{R_{oD}^2}{R_{oD}^2-1}(\mathrm{Bn}\ln R_{oD} + 1)\left(\frac{1}{r_D^2}-1\right)\right]_P \tag{A34}$$

The two flow scales are also geometrically similar, i.e., $R_{oD,M} = R_{oD,P}$. Thus Eq. (A34) can be reduced to

$$\mathrm{Bn}_M = \mathrm{Bn}_P \tag{A35}$$

Substitution of the expression for Bingham's number from Eq. (A26) into Eq. (A35) yields

$$\frac{\tau_{0,M}}{\tau_{0,P}} = \frac{K_M \omega_M}{K_P \omega_P} \tag{A36}$$

Eq. (A36) is consistent with the scaling equations for the Bingham-Plastic fluid in the current work.

References

[1] Nouri, J. M., Whitelaw, J. H., "Flow of Newtonian and non-Newtonian fluids in a concentric annulus with rotation of the inner cylinder," J. Fluids Eng. 116: 821–827, 1994.

[2] Lueptow, R. M., Docter, A., Min K., "Stability of axial flow in an annulus with a rotating inner cylinder," Phys. Fluids Fluid Dynam. 4: 2446–2455, 1992.

[3] Escudier, M. P., Gouldson, I. W., Oliveira, P. J., Pinho, F. T., "Effects of inner cylinder rotation on laminar flow of a Newtonian fluid through an eccentric annulus," Int. J. Heat Fluid Flow 21: 92–103, 2000.

[4] Tachibana, M., Kawabata, N., Genno, H., "Steady laminar flow of power-law fluids in the inlet region of rectangular ducts," J. Rheol. 30: 517–538, 1986.

[5] Mannheimer, R. J., "Laminar and turbulent flow of cement slurries in large diameter pipe: a comparison with laboratory viscometers," J. Rheol. 35: 113–133, 1991.

[6] Volarovich, M. P., Gutkin, A. M., "Flow of plastic-viscoplastic material between two parallel flat-walls and in annular space between two coaxial tubes," J. Tech. Phys. 16: 321–328, 1946.

[7] Fredrickson, A. G., Bird, R. B., "Non-Newtonian flow in annuli," Ind. Eng. Chem. 50: 347–352, 1958.

[8] Hanks, R. W., Larsen, K. M., "The flow of power-law non-Newtonian fluids in concentric annuli," Ind. Eng. Chem. Fundam. 18: 33–35, 1979.

[9] Luo, Y., Peden, J. M., "Flow of drilling fluids through eccentric annuli," SPE Annual Technical Conference and Exhibition, Dallas, Texas, USA, September 1987.

[10] Laird, W. M., "Slurry and Suspension Transport," Ind. Eng. Chem. Res. 49: 138–141, 1957.

[11] Deterre, R., Nicoleau, F., Lin, Q., Allanic, N., Mousseau, P., "The flow of power-law fluids in

concentric annuli: a full analytical approximate solution," J. Non-Newton. Fluid Mech. 285: 104392, 2020.
[12] Escudier, M. P., "Fully developed laminar flow of purely viscous non-Newtonian liquids through annuli, including the effects of eccentricity and inner-cylinder rotation," Int. J. Heat Fluid Flow 23: 52–73, 2002.
[13] Azouz, I., Shirazi, S. A., Pilehvari, A., Azar, J. J., "Numerical simulation of laminar flow of yield-power-law fluids in conduits of arbitrary cross-section," J. Fluids Eng. 115: 710–716, 1993.
[14] Guckes, T. L., "Laminar flow of non-Newtonian fluids in an eccentric annulus," J. Energy Resour. Technol. 97: 498–506, 1975.
[15] Haciislamoglu, M., Langlinais, J., "Non-Newtonian flow in eccentric annuli," J. Energy Resour. Technol. 112: 163–169, 1990.
[16] Hussain, Q. E., Sharif, M. A. R., "Analysis of yield-power-law fluid flow in irregular eccentric annuli," J. Energy Resour. Technol. 120: 201–207, 1998.
[17] Dosunmu, I. T., Shah, S. N., "Annular flow characteristics of pseudoplastic fluids," J. Energy Resour. Technol. 137: 042903, 2015.
[18] Dosunmu, I. T., Shah, S. N., "Pressure drop predictions for laminar pipe flow of Carreau and modified power law fluids," Can. J. Chem. Eng. 93: 929–934, 2015.
[19] Filip, P., David, J., "Poiseuille flow of power-law fluids in concentric annuli-limiting cases," 6th International Conference on Heat Transfer, Fluid Mechanics and Thermodynamics, Pretoria, South Africa, June 30, 2008.
[20] Tang, M., Ahmed, R., He, S., "Modeling of yield-power-law fluid flow in a partially blocked concentric annulus," J. Nat. Gas Sci. Eng. 35: 555–566, 2016.
[21] Ortega-Avila, J. F., Pérez-González, J., "Axial annular flow of a viscoplastic microgel with wall slip," J. Rheol. 60: 503–515, 2016.
[22] Wan, S., Morrison, D., Bryden, I. G., "The flow of Newtonian and inelastic non-Newtonian fluids in eccentric annuli with inner-cylinder rotation," Theor. Comput. Fluid Dyn. 13: 349–359, 2000.
[23] Erge, O., Ozbayoglu, M. E., Miska, S. Z., Yu, M., Takach, N., Saasen, A., May, R., "Effect of drillstring deflection and rotary speed on annular frictional pressure losses," J. Energy Resour. Technol. 136: 1–10, 2014.
[24] Escudier, M. P., Oliveira, P. J., Pinho, F. T., "Fully developed laminar flow of purely viscous non-Newtonian liquids through annuli, including the effects of eccentricity and inner-cylinder rotation," Int. J. Heat Fluid Flow, 23: 52–73, 2002.
[25] Vieira Neto, J. L., Martins, A. L., Ataíde, C. H., Barrozo, M. A. S., "Non-Newtonian flows in annuli with variable eccentric motion of the inner tube," Chem. Eng. Technol., 35: 1981–1988, 2012.
[26] Gray, J. D., Owen, I., Escudier, M. P., "Dynamic scaling of unsteady shear-thinning non-Newtonian fluid flows in a large-scale model of a distal anastomosis," Exp. Fluids. 43: 535–546, 2007.
[27] Barenblatt, G. I., Scaling, Self-similarity, and Intermediate Asymptotics, Cambridge University Press, 1996.
[28] Aadnoy, B., Cooper, I., Miska, S. Z., Mitchell, F., Payne, M. L., "Advanced drilling and well technology," Society of Petroleum Engineers Conference, Richardson, TX, USA, 2009.
[29] Chhabra, R. P., Richardson, J. F., Non-Newtonian Flow and Applied Rheology: Engineering Applications, Butterworth-Heinemann, 2011.
[30] Wang, N., Liu, H., Zhang, C., "Deformation and breakup of a confined droplet in shear flows with power-law rheology," J. Rheol. 61: 741–758, 2017.
[31] Hanks, R. W., "The laminar-turbulent transition for fluids with a yield stress," AIChE J. 9: 306–309, 1963.
[32] Csizmadia, P., Hős, C., "Predicting the friction factor in straight pipes in the case of Bingham plastic and the power-law fluids by means of measurements and CFD simulation," Period. Polytech. Chem. Eng. 57: 79–83, 2013.
[33] Taylor, A. J., Wilson, S. D. R., "Conduit flow of an incompressible, yield-stress fluid," J. Rheol. 41: 93–101, 1997.
[34] Piercy, N. A. V., Hooper, M. S., Winny, H. F. "Viscous flow through pipes with core," London Edinburgh Philos. Mag. J. Sci. 15: 647–676, 1933.
[35] Chatzimina, M., Gerogiou, G., Alexandrou, A., "Wall shear rates in circular Couette flow of a Herschel-Bulkley fluid," Appl. Rheol. 19: 34288, 2009.
[36] Caenn, R., Darley, H. C. H., Gray, G. R., Composition and Properties of Drilling and Completion Fluids, Gulf Professional Publishing, 2011.
[37] Bourgoyne, A. T., Millheim, K. K., Chenevert, M. E., Young, F. S., "Applied Drilling Engineering," Society of Petroleum Engineers Conference, Richardson, TX, USA, 1991.
[38] Ovarlez, G., Mahaut, F., Deboeuf, S., Lenoir, N., Hormozi, S., Chateau, X., "Flows of suspensions of particles in yield stress fluids," J. Rheol. 59: 1449–1486, 2015.
[39] Deb, K., Multi-objective Optimization, Search Methodologies, Springer, 2014.
[40] Vanderbei, R. J., Linear Programming, Foundations and Extensions, Springer, 2015.